We are IntechOpen, the world's leading publisher of Open Access books Built by scientists, for scientists

4,800
Open access books available

122,000
International authors and editors

135M
Downloads

Our authors are among the

154
Countries delivered to

TOP 1%
most cited scientists

12.2%
Contributors from top 500 universities

CLARIVATE ANALYTICS BOOK CITATION INDEX INDEXED

WEB OF SCIENCE™

Selection of our books indexed in the Book Citation Index in Web of Science™ Core Collection (BKCI)

Interested in publishing with us?
Contact book.department@intechopen.com

Numbers displayed above are based on latest data collected.
For more information visit www.intechopen.com

Chapter 3

Engineering of Novel Proteinoids and PLLA-Proteinoid Polymers of Narrow Size Distribution and Uniform Nano/Micro-Hollow Particles for Biomedical Applications

Michal Kolitz-Domb and Shlomo Margel

Additional information is available at the end of the chapter

http://dx.doi.org/10.5772/59626

1. Introduction

Proteinoids, polymers made of amino acids by thermal condensation polymerization, are unique synthetic polymers studied by Fox and coworkers [1-7]. When present in certain concentrations in aqueous solutions, the proteinoids form small microscopic structures called "proteinoid microspheres" or protocells [4]. The proteinoid, made of most common amino acids, goes through a self-assembly process in specific conditions, as some of the amino acids incorporated into proteinoid chains are more hydrophobic than others, thus proteinoids cluster together like droplets of oil in water [5-7].

The amino acids, either natural or synthetic, are polymerized by step-growth polymerization in a special procedure discovered by Fox and Harada [8-12]. The procedure involves heating amino acids until they melt at first, and then the polymerization is initiated to give the proteinoid. The polymerization takes place at a relatively high temperature (e.g., 180 °C), in absence of a solvent or a catalyst, and in an inert atmosphere. The accepted explanation of this polymerization process is that glutamic acid is used as a solvent for the other monomers, as it is condensed into pyroglutamic acid. The pyroglutamic acid initiates the polymerization with the rest of the present amino acids [11-14]. A brief description of the polymerization process is shown in Figure 1.

An important advantage in using biodegradable polymers bearing one or more stereogenic centers- optically active polymers- is the high variety of features they offer, when used as carriers for drug delivery systems [15]. This study is intended to broaden the scope of

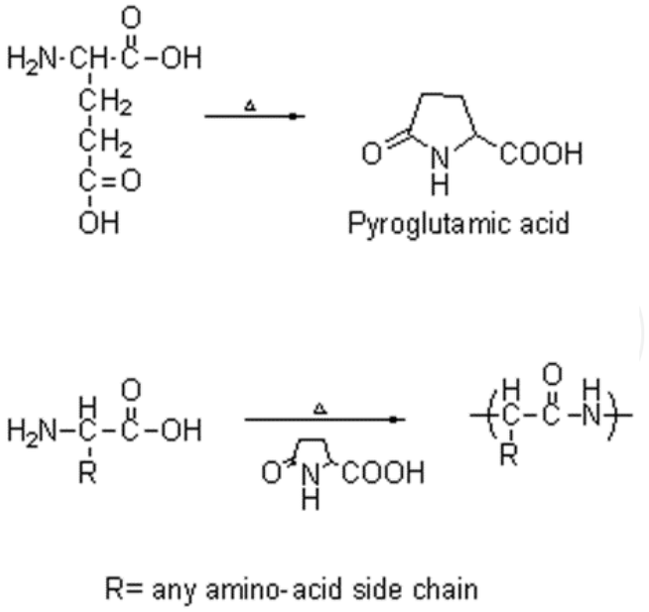

Figure 1. Thermal polymerization of amino acids through pyroglutamic acid catalysis.

biodegradable polymers by synthesizing new proteinoids carrying various stereogenic centers. The main goal is to provide a large choice of biodegradable proteinoids with predetermined characteristics, while using amino acids as building blocks. Hence, the new selection is based on chiral building blocks carrying positive/negative charge, hydrophilic/hydrophobic nature or any desired combination of the above [16]. Homopolymers, random copolymers and block-copolymers of two amino acids or more can be designed and synthesized, presenting thereby new proteinoid materials with specific, desired nature. The large variety of amino acids, either natural or synthetic, makes it possible to obtain a large library of different proteinoids, by simply changing the amino acids ratios. One proteinoid is completely different from another, by the fact that they are made of different amino acid monomers. This fact provides each proteinoid special features, and possibly influences the character of particles made from it [17-20].

Up until now, most, if not all, of the reported proteinoids in the literature were synthesized from at least four amino acids and possessed relatively low molecular weights [21,22]. Thus, high molecular weight proteinoids of narrow size distribution made of two to three natural amino acids, along with proteinoids containing poly(L-lactic acid) (PLLA) segments are presented in this study. Furthermore, the study presents NIR fluorescent proteinoid-based particles, which can be used for colon cancer detection. Some of the methods used have been published in a previous work [23].

2. Incorporation of poly(L-lactic acid) into the proteinoid backbone

Poly(lactic acid) or PLA is the thermoplastic aliphatic polyester of lactic acid, derived from renewable sources. It is the one of the most important bioplastics in the world in terms of

consumption volume. PLA can be processed by extrusion, injection molding, film and sheet casting, and spinning, providing access to a wide range of materials and applications. Two racemic structures of PLA, the L form and the D form, are known as PLLA and PDLA, respectively [24].

PLA is already used in many biomedical applications, as it is able to degrade into innocuous lactic acid and is very safe [25-29]. Medical implants made of PLA and approved by the FDA are anchors, screws, plates, pins, rods, and as a mesh. Depending on the specific type used, the implants degrade inside the body within 6 to 24 months. The strength characteristics of PLA and PLLA implants is well documented [30,31].

PLA can also be used as a compostable packaging material, either cast, injection molded, or spun. Also, cups, bags, hygene products and diapers have been made from PLA [32].

3. Proteinoid microspheres

After preparation, the crude proteinoids can self-assemble to form micro- and nano-sized particles [33, 34]. As opposed to polystyrene microparticles, for example, which are formed during the polymerization process of styrene in the presence of a surfactant [35], the proteinoid particles are formed through a self-assembly process. This process is completed only after the polymerization itself. The procedure involves either dissolving the dried crude proteinoid in water by heating and then cooling slowly,[36] or by pH changes of the proteinoid solution in water [37]. This way, particles of the size range of several nanometers to 10 μm may be formed [38].

The idea standing behind the unique self-assembly process lies in the existence of many functional groups as a part of the random polymer backbone. The preparation of proteinoid microspheres does not require the addition of any toxic cross-linking agents or surfactants. The conversion of the polypeptidic proteinoid solution into particles with a slight change of the environment involves a complex process of functional group changes occurring in the polymer. The great amount of carboxylates in the backbone, or aminium ions when dealing with a lysine-rich proteinoid, cause the solubility of the proteinoid in certain conditions and insolubility in the reverse conditions [39]. The hydrophobic portions of the proteinoid are assembled within the particle matrix, and the carboxylic acid moieties are exposed, as illustrated in Figure 2 [40].

When the self-assembly procedure is done in the presence of a suitable molecule such as drug or dye, a proteinoid particle containing the molecule is formed [41]. The proteinoids may be used to encapsulate materials such as drugs for drug delivery purposes, e.g. for the oral delivery of methotrexate [40], Hydroxyapetite [42], Cholesterol [37] and for diagnostics [21,43-48].

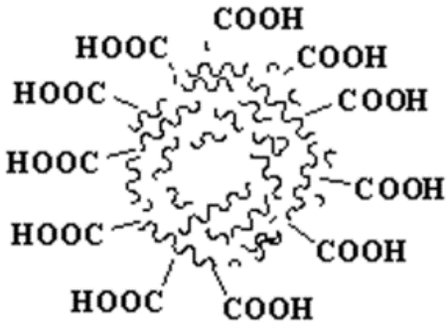

Figure 2. Schematic representation of the self-assembled proteinoid particles. Hydrophobic moieties are represented by scribbled lines. When lysine is also a part of the proteinoid, as in Prot5-7, some carboxyl groups are exchanged with amine groups.

4. Preparation of proteinoids by thermal condensation polymerization

L-glutamic acid was heated to the molten state (180°C) in an oil bath, under nitrogen atmosphere. The molten mass was stirred at 180°C for 30 min. To this, different contents of additional L-amino acids were added to give a total monomer weight of 5-5.01 g, as specified in Table 1, and kept at 180°C under nitrogen. The mixture was mechanically stirred at 150 rpm for 3 h. The product is a highly viscous orange-brown paste, which hardens to give a glassy mass when cooled to room temperature. Then, water (10 mL) was added to the crude product, and the mixture was stirred for 20 min. The solution was then intensively dialyzed through a cellulose membrane (3500 Da MWCO) against distilled water. The content of the dialysis tube was then lyophilized to obtain a yellow-white proteinoid powder.

Polymer	Amino acid content (g)a				
	L-Glu	L-Asp	L-Lys	L-Phe	PLLA
Prot1	5	-	-	-	-
Prot2	2.5	2.5	-	-	-
Prot3	2.5	-	-	2.5	-
Prot4	1.25	2.5	-	1.25	-
Prot5	1.67	1.67	1.67	-	-
Prot6	1.67	-	1.67	1.67	-
Prot7	1.25	-	2.5	1.25	-
Prot8	2.25	-	-	2.25	0.5

Table 1. Amino acid content of the different proteinoids. [a]In all proteinoids made by thermal condensation polymerization the total monomer content was 5-5.01 g; [b]made by microwave-assisted polymerization.

4.1. Polymerization kinetics study at different temperatures

Polymerization kinetics was studied by collecting proteinoid samples from the reaction vessel at different time periods of the polymerization at 180, 190 and 200°C. The samples

were then analyzed by both ninhydrin test for the determination of the primary amine groups content and Biuret test for the determination of the amide groups content of the various proteinoids [49]. The results shown in Figure 3 refer to the synthesis of Prot3, consisting of L-glutamic acid and L-phenylalanine. Similar results were observed for the other systems, Prot1-8, as well. It can be seen that at all temperatures, the polymerization takes place mainly over the first 100 min. After that, both ninhydrin (A) and Biuret (B) tests show no significant drop of the Ninhydrin signal indicating the amount of free amines or rise of the peptide bonds shown by the Biuret signal. This figure also shows that as the temperature of the reaction was raised, the rate of the reaction increased. However, the preferred reaction temperature is 180°C, as the yield of the reaction is higher since the amino acids decompose faster at the higher temperatures.

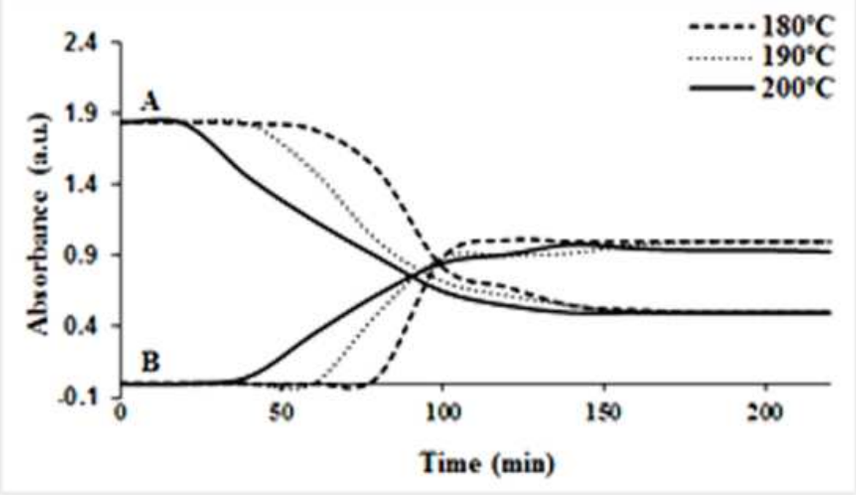

Figure 3. Thermal polycondensation kinetics of (L)glutamic acid and (L)phenylalanine to yield Prot3 at different temperatures by two tests: ninhydrin test (A) and Biuret test (B).

5. Proteinoid analysis and characterization

The molecular weights and polydispersity index of the dried crude proteinoids were determined using Gel Permeation Chromatography (GPC) consisting of a Waters Spectra Series P100 isocratic HPLC pump with an ERMA ERC-7510 refractive index detector and a Rheodyne (Coatati, CA) injection valve with a 20 μL loop (Waters, MA). The samples were eluted with super-pure HPLC water through a linear BioSep SEC-s3000 column (Phenomenex) at a flow rate of 1 mL/min. The molecular weights were determined relative to poly(ethylene glycol) standards (Polymer Standards Service-USA, Silver Spring, MD) with a molecular weight range of 100-450000 Da, using Clarity chromatography software. The optical activities of the proteinoids were determined using a PE 343 polarimeter (PerkinElmer). All of the measurements were done in water, at 589 nm at 25°C. Table 2 shows the characteristic molecular weights, polydispersity and optical activity of the prepared proteinoids.

Proteinoid[a]	Mw (Da) b	Mn (Da) b	Mp (Da) b	PDIc	Optical Activity [α]D25°C (°)d
Prot1	26250	11300	11320	2.32	+6.5
Prot2	181540	144940	195300	1.25	-4.4
Prot2[e]	500240	497280	503070	1.01	+8.1
Prot3	164930	138250	158740	1.19	-9.0
Prot4	87660	84410	85250	1.04	-3.3
Prot5	195080	165870	191440	1.17	-7.4
Prot6	190390	163290	204050	1.16	-15.1
Prot7	72260	56880	42870	1.27	+2.8
Prot8	168300	156600	136800	1.07	-4.6

Table 2. Mw, Mn, Mp, PDI and optical activity of the various proteinoids.[a]The proteinoids were prepared at 180°C according to section 3.2.1; [b]molecular masses were measured by GPC, Mp is the molecular mass at the peak; [c]PDI is the polydispersity index, given by Mw/Mn; [d]specific optical rotation (c=1, in H_2O, at 25°C); [e]made by microwave-assisted polymerization.

Table 2 indicates relatively low PDI values for the obtained proteinoids. This is unexpected since the polycondensation of the various amino acids is random and step-growth polymerization processes, as in the present case, result usually in very broad size distribution polymers [50]. The highest PDI (2.32) was observed for Prot1, composed of the single amino acid L-glutamic acid, while the PDIs of the other proteinoids composed of at least 2 amino acids were ranging between 1.01 and 1.27. All of the thermally-made proteinoids have relatively high molecular masses of 26-195 kDa. This indicates that the polymerization procedure by thermal heating used here provides relatively long polymer chains. This fact may serve as an advantage for different uses later, since polymers with such high molecular weights are usually mechanically stronger and resemble natural proteins. Table 2 indicates that the lowest molecular weight was observed for the proteinoid composed of the single amino acid L-glutamic acid (Prot1) and the highest one for the proteinoid composed of L-glutamic acid, L-aspartic acid and L-lysine (Prot 5). Prot2, which was synthesized by microwave-assisted polymerization, reached an abundantly higher molecular weight. In this procedure, a 500 kDa proteinoid chain was prepared, about twice the size of the regular thermal proteinoid. This kind of procedure gives better yield over 60 min, compared to the 3 h needed usually. It can be used further for higher molecular weights and more rigid proteinoids. However, unfortunately, this kind of proteinoid does not self-assemble into spherically-shaped particles.

As further indicated from Table 2, all of the proteinoids exhibit optical activity, although the amino acid monomers are known to racemize during the thermal process [51]. This fact can become a benefit later in the design of a stereospecific drug carrier, for example.

Fourier Transform Infra-Red (FTIR) measurements of the crude proteinoids were done by the Attenuated Total Reflectance (ATR) technique, using Bruker ALPHA-FTIR QuickSnapTM sampling module equipped with Platinum ATR diamond module. All proteinoids showed characteristic peaks of NH stretching at 3360 and 2990 cm-l, amide CO stretching at 1565 cm-1,

http://dx.doi.org/10.5772/59626

an amide NH bending band at 1450 cm-1 and CO bending at 500-700 cm-1. A representative spectrum of Prot3 is shown in Figure 4.

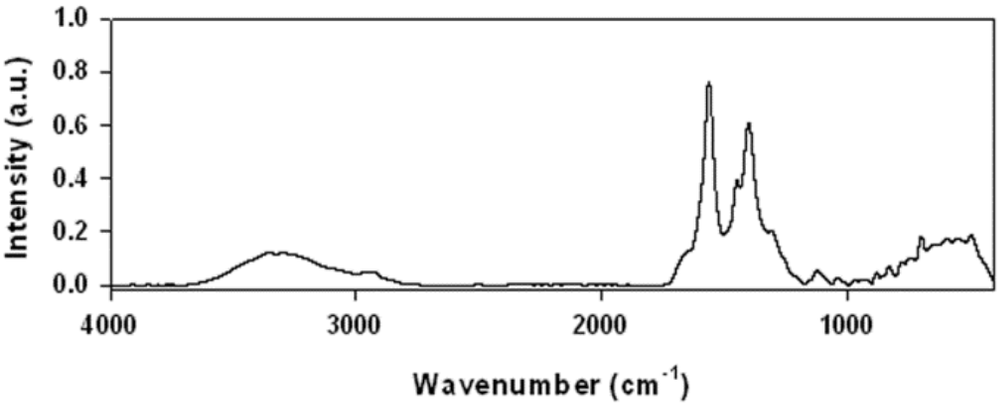

Figure 4. FTIR spectrum of Prot3.

The thermal behavior of the proteinoids was determined using Differential Scanning Calorimetry (DSC) and Thermo Gravimetric Analysis (TGA) with a TGA/DSC 1 STARe system (Mettler Toledo, Switzerland). The samples were heated between 25 - 400 °C at a rate of 10°C/min under nitrogen atmosphere. The results are shown in Table 3.

Polymer	Tm(°C)a	ΔHm (J/g)a	Tdec (°C)b	Weight loss (%) at 400°Cb
Prot1	102	-300.7	300	55
Prot2	89	-428.7	297	57
Prot3	103	-174.9	341	54
Prot4	217	-183.4	330	25
Prot5	78	-251.5	339	57
Prot6	241	-90.1	373	47
Prot7	246	-139.4	385	64
Prot8	117	-420.5	268	47
PLLA[c]	150	-57.2	349	90

Table 3. Thermal properties of proteinoids produced by thermal polymerization. [a]Tm and ΔHm were measured by DSC; [b]Tdec (temperature of decomposition) was measured by TGA/DSC and refer to the exothermal peak in DSC, [c]commercial PLLA 2000 Da parameters were measured similar to the made proteinoids.

The melting temperatures of the different proteinoids range between 78-246°C. The wide range of temperatures derives from the difference in the monomeric units used in each proteinoid. When using phenylalanine, as in Prot3, 4, 6 and 7, the resulted proteinoid gains significant rigidity in the overall structure, due to the aromatic rings which allow pi-stacking. Hence, these proteinoids melt at higher temperatures. When PLLA is incorporated into the proteinoid, as

in Prot8 compared to Prot3, the Tm rises mildly (103°C and 117°C, respectively), due to the presence of 2000 Da rigid polymer chains in the overall proteinoid structure.

The TGA/DSC measurements of the proteinoids show decomposition temperatures of 268-385°C. Most proteinoids lose at this temperature range around 50% of their weight The decomposition measured at 400°C of most proteinoids is between 47-64%, except Prot4 (25%). Pure PLLA decomposes at 349°C almost completely (90% weight loss). Prot8, composed of PLLA segments (10% of the total monomer), has the lowest decomposition temperature of all proteinoids (268°C). This can be explained by the non-uniformity of the structure of the whole proteinoid due to the inserted segments of 2000 Da PLLA within the random segments of polymerized amino acids.

The content of free carboxyl groups in the synthesized proteinoids is an essential factor in determining their solubility in different media, thus helping to understand their stability at different sites in the human body with different pHs. In order to determine the free carboxyl groups in the synthesized proteinoids, a titrimetric method was carried out [40]. Briefly, to a known quantity of dry proteinoid, a known excess of 0.05 N NaOH was added, followed by the addition of 37% formaldehyde solution. The unreacted NaOH was back-titrated with standard 0.05 N HCl. A blank titration was also performed. In addition, human serum albumin (HSA) was titrated for comparison. Table 6 indicates the carboxyl group contents of the synthesized proteinoids, showing higher values of 80-155 mmol/g compared with albumin. This is true also in Prot5-7, where lysine is also a part of the polymer. Moreover, aspartic and glutamic acid moieties in the proteinoids, along with lysine, impart the hydrophilic nature of the whole proteinoid. The biodegradability rate of various amino acid polymers increases with their hydrophilicity [40]. Therefore, it is more appropriate to choose these proteinoids as ideal biomaterials for drug delivery applications.

Polypeptide	[Carboxyl groups] (mmol/g)
Albumin	56
Prot1	150
Prot2	155
Prot3	90
Prot4	122
Prot5	88
Prot6	87
Prot7	80
Prot8	102

Table 4. Carboxyl group content in the proteinoids and albumin.

5.1. Incorporation of poly(L-lactic acid) into the proteinoids

In order to effect the chemical and physical properties of the product, a thermal polymerization of L-glutamic acid and L-phenylalanine was carried out in the presence of low molecular

weight poly(L-lactic acid) (PLLA, 2000 Da). The proteinoid-PLLA (Prot8) consists of 2.25 g of each amino acid and 0.5 g of PLLA. After polymerization, it was washed, dried and characterized as described earlier. The characterization of Prot8 is included in the tables above.

6. Preparation and characterization of the proteinoid nano/micro-particles by a self-assembly process

Proteinoid particles were prepared by a self-assembly mechanism. Briefly, 100 mg of the dried proteinoid were added to 10 mL 10-5N NaCl solution. The mixture was then heated to 80°C until the crude proteinoid dissolves completely. Proteinoid particles were then formed by removal of the heating and leaving the mixture to cool to room temperature.

Hydrodynamic diameter and size distribution of the particles dispersed in double distilled (DD) water were measured at room temperature with a particle DLS analyzer model Nanophox (SympatecGmbH, Germany).

Dried particle size and size distribution were measured with a Scanning Electron Microscope (SEM). SEM pictures were obtained with a JEOL, JSM-840 Model, Japan. For this purpose, a drop of dilute particle dispersion in distilled water was spread on a glass surface, and then dried at room temperature. The dried sample was coated with carbon in vacuum before viewing under SEM. The average particle size and distribution were determined by the measurement of the diameter of more than 200 particles with image analysis software (Analysis Auto, Soft Imaging System GmbH, Germany). Figure 5 exhibits the proteinoid particles made from self-assembly of Prot8. The procedure produced spherical proteinoid particles of 103 ± 11 nm hydrodynamic diameter and 70 ± 15 nm dry diameter. The dry diameter of the proteinoid particles is illustrated by the typical SEM photomicrograph shown in Figure 5A. The hydrodynamic diameter of these particles dispersed in water is illustrated by the typical light scattering measurement shown in Figure 5B. The difference in the particle size between the SEM and the light scattering measurements is probably due to the fact that SEM measurements determine the dry diameter, whereas light scattering measurements take into account the hydrated water layers adsorbed onto the particle's surface.

The density of the particles was determined by pycnometry [52]. Briefly, dry pre-weighed particles were put in a calibrated pycnometer, which was then filled with water. The density of the sample can then be calculated from the known density of the water, the weight of the pycnometer filled only with water, the weight of the pycnometer containing both the sample and water, and the weight of the sample, as described in the literature [52]. Density measurements indicated that all proteinoid particles possess a very low density, ranging from 0.001 to 0.014 g/mL indicating that the particles formed are probably hollow, as already indicated for the proteinoids prepared by Fox et al [6,38]. The hollow nature of the particles is significantly important for applications such as ultrasound imaging agents, drugs and dyes encapsulation, controlled released, etc.

As suggested in our and in previous studies, the proteinoid forms particles of different sizes according to the nature of its surrounding. The hydrophobic portions of the crude proteinoid

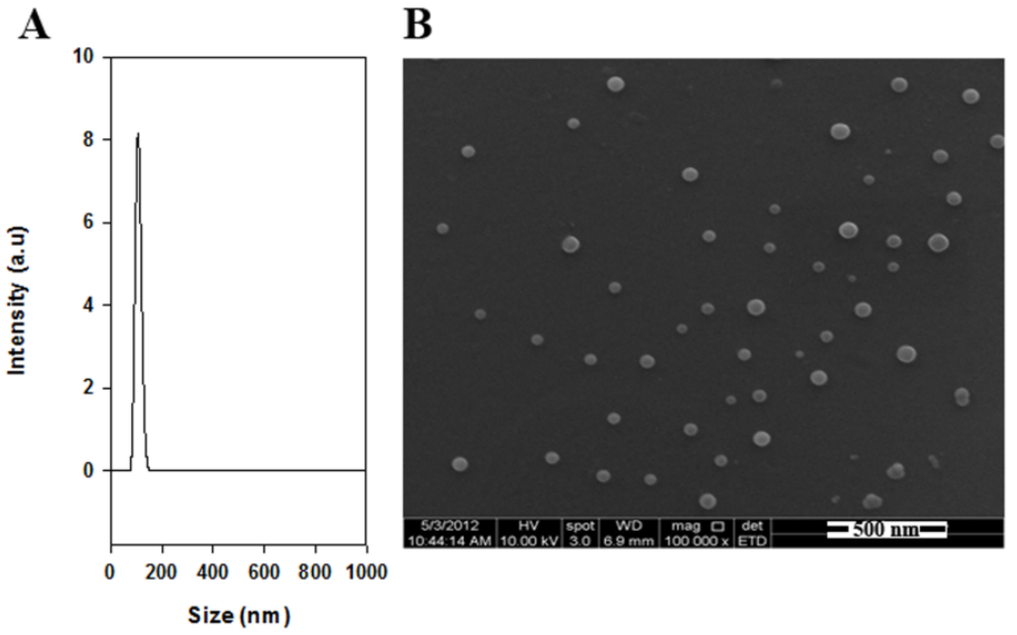

Figure 5. Hydrodynamic size histogram (A) and SEM image (B) of Prot8 particles.

are assembled within the particle matrix, while the polar hydrophilic groups (carboxyl and amines) are exposed to the aqueous environment, as illustrated before in Figure 2 [40].

6.1. Particle stability in storage conditions

Proteinoid particles aqueous dispersions (1 mg/mL) were put in a refrigerator at 4°C for 6 months. Samples were taken at different time periods, filtered through a centrifugation tube (Vivaspin 3000 Da MWCO) and the filtrate was checked by UV at 200-210 nm, to find aqueous soluble proteinoid. Also, the particle aqueous dispersions were checked by Nanophox for their size and size distribution. In order to check the particle stability after drying, the particles were lyophilized to dryness and then dispersed in an aqueous phase to their original concentration. The samples size and size distribution were then rechecked by Nanophox. Overall, the proteinoid particles remain in the same size after 6 months in storage at 4°C. Also, the degradation and/or dissolution of the proteinoid particles in the aqueous continuous phase was tested by the filtration centrifugation method and resulted in negative results in the filtrate, meaning no degradation or dissolution occurs at this temperature over 6 months. When lyophilized to dryness, the proteinoid particles can be redispersed in water completely while the particle size and size distribution remain the same. This means that the particles can be stored as a freeze-dried powder as well, and redispersed when needed, without the need to add cryoprotectants as mentioned in the literature [53].

6.2. Cytotoxicity of the proteinoid particles

In vitro cytotoxicity of the proteinoid particles was tested by using human colon adenocarcinoma LS174T cancer cell line. The tests were done on Prot2, Prot4, Prot5, Prot7 and Prot8. The

cell line is adherent to the used culture dishes. LS174T cells were grown in MEM that was supplemented with 10% heat-inactivated fetal bovine serum (FBS), 1% glutamine and 1% penicillin/streptomycin. Cells were screened to ensure they remained mycoplasma-free using Mycoplasma Detection Kit [54]. Cell cytotoxicity was assessed by measuring the release of cytoplasmic lactate dehydrogenase (LDH) into cell culture supernatants. LDH activity was assayed using the Cytotoxicity Detection Kit according to the manufacturer's instructions [55]. Cells (3×105 cells per well) were seeded and grown to 90–95% confluency in 24 well plates before treatment with the proteinoid particles. Cell cultures that were not exposed to the particles were included in all assays as negative controls. Cell cultures that were treated with 1% Triton-x-100 were used as positive controls. To test if the particles can interact with LDH kit compounds, cell cultures were exposed to a mixture containing maximal nano/micro-particles concentration dispersed in PBS and 1% Triton-x-100. The proteinoid particles were freshly dispersed in PBS (1.25 and 2.5 mg/mL) and then added to the 95% confluent cell culture in culture medium. The cell cultures were further incubated at 37°C in a humidified 5% CO2 incubator and then checked for cellular cytotoxicity at intervals of 24h. The percentage of cell cytotoxicity was calculated using the formula shown in the manufacturer's protocol [55]. All samples were tested in tetraplicates.

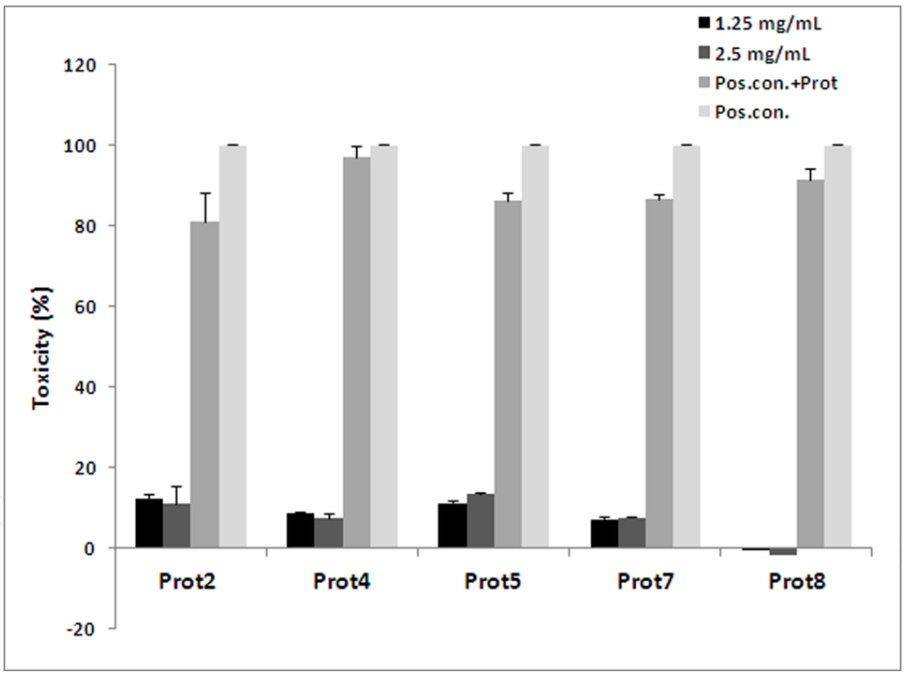

Figure 6. Cytotoxic effect of the proteinoid particles on colon adenocarcinoma LS174T cells measured by the LDH assay. Cells (3×10^5) were incubated for 24 and 48 h with the proteinoid particles dispersed in PBS (1.25 mg/mL and 2.5 mg/mL) according to section 3.2.5.8. Cells were incubated with Triton-x-100 1% as positive control (100% toxicity). In addition, cells were incubated with Triton-x-100 1% and each one of the proteinoids to revoke any interaction. Untreated cells (negative control) were similarly incubated. Each bar represents mean ± standard deviations of 4 separate samples.

When tested by the LDH quantitative assay, Prot2, 4, 5, 7 and 8 particles dispersed in PBS at concentrations of 1.25 and 2.5 mg/mL had none, or minor cytotoxic effect on the human colon adenocarcinoma cell line LS174T (Figure 6). Treatment of the cells with Prot2 and Prot5

particles at both concentrations produced the highest LDH levels (up to 13% toxicity), when compared to untreated (blank) cells, indicating minor toxicity of these proteinoids to this cell line. Prot8 had the lowest cytotoxic effect on the cells treated with both concentrations, almost zero toxicity. This proteinoid is therefore the most suitable for treating cells, considering its low toxicity.

7. NIR flourescent proteinoid-PLLA particles

7.1. Synthesis of the NIR fluorescent Prot8 particles

The optimal Prot8 particles were used to encapsulate ICG, a well-known NIR dye already in use in medical diagnostics. The NIR fluorescent particles were prepared by self-assembly of the crude Prot8, in the presence of ICG. Briefly, 100 mg of the dried fabricated Prot8 were resuspended in 10 mL of 10-5N NaCl solution. The mixture was then heated to 80°C while stirring for 15 min. To this solution, 1 mg (1% of the proteinoid polymer) of ICG was added. The mixture was then removed from the hot plate and was allowed to return to room temperature. During the cooling process hollow particles were formed and precipitated from solution. The obtained NIR fluorescent particles dispersed in water were then dialyzed versus 4 L of 10-5 NaCl aqueous solution overnight at room temperature.

7.2. Determination of the encapsulated ICG concentration in the NIR fluorescent Prot8 particles

A calibration curve of free ICG was obtained by measuring the integrals of absorbance peaks of standard solutions (0.5–10 μg/mL) in PBS, at wavelengths 630–900 nm. The concentration of the encapsulated ICG was determined by measuring the integral of the absorbance spectrum at 630-900 nm of a 1 mg/mL dispersion of the NIR fluorescent particles in PBS. An estimation of encapsulated ICG per mg of particles was determined according to the calibration curve.

7.3. Characterization of the NIR fluorescent Prot8 particles

Hydrodynamic and dry particle size and size distribution were determined by DLS and SEM, as mentioned above. For the SEM study, the diameter of more than 200 particles with image analysis software (AnalySIS Auto, Soft Imaging System GmbH, Germany). The self-assembly procedure produced spherical proteinoid particles of 145 ± 20 nm hydrodynamic diameter and 70 ± 15 nm dry diameter, as shown in Figure 7. The hydrodynamic diameter of these particles dispersed in water is illustrated by the typical light scattering measurement shown in Figure 7A. The dry diameter of the proteinoid particles is illustrated by the typical SEM photomicrograph shown in Figure 7B.

In addition, absorbance spectra were obtained using a Cary 100 UV-Visible spectrophotometer (Agilent Technologies Inc.). Excitation and emission spectra were recorded using a Cary Eclipse spectrofluorometer (Agilent Technologies Inc.). As indicated in Figure 8, no shift of absorbance of the ICG after encapsulation is observed compared to that of the free ICG.

http://dx.doi.org/10.5772/59626

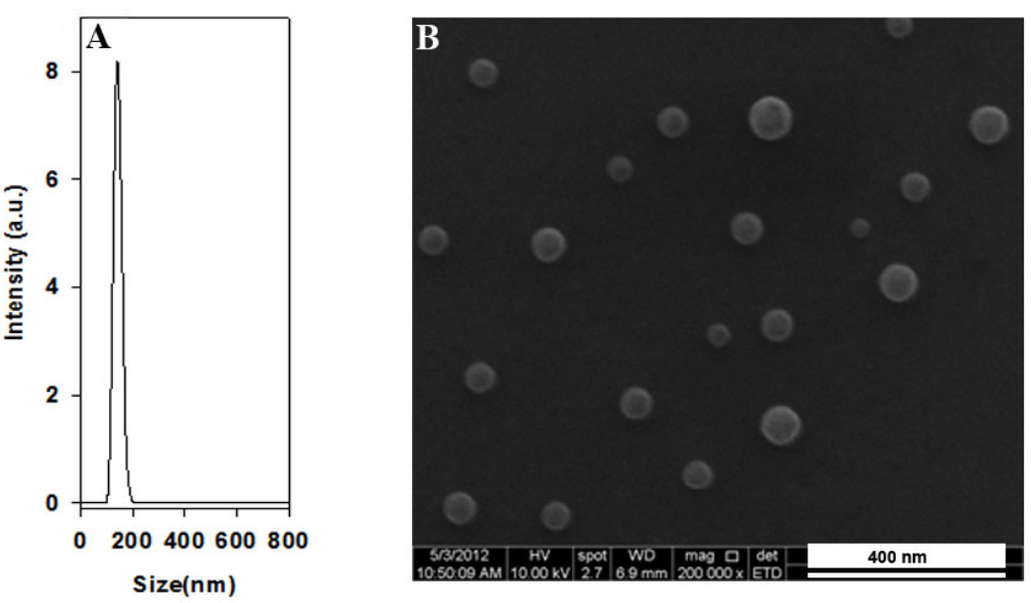

Figure 7. Hydrodynamic size histogram (A) and SEM image (B) of the P(EF-PLLA) NIR fluorescent nanoparticles.

However, due to the dye encapsulation process, the maximal absorbance peak of the free ICG changed from 779 nm to 718 nm, probably since the ICG molecules get close to each other inside the nanoparticle interior and aggregation of the dye may occur causing this change in absorption peaks [56,57]. Furthermore, a 12 nm blue-shift of the emission spectrum of the NIR fluorescent particles compared to the free dye in solution is also observed.

The estimation of encapsulated ICG showed that the complete quantity of ICG used in the encapsulation procedure was encapsulated within the Prot8 nanoparticle interior. Following particle formation, leakage of the encapsulated ICG into PBS not-containing and containing 4% albumin at room temperature was not observed, indicating that the dye is strongly associated within the Prot8 particles, probably due to physical interactions between the dye and the polymer hydrophobic portions assembled in the core of the particles.

As suggested before, the proteinoid forms particles of different sizes according to the nature of its surrounding [40]. When discussing Prot8, the hydrophobic portions, in this case mainly the PLLA segments and the aromatic rings of the phenylalanine portion are assembled within the particle matrix, while the polar hydrophilic groups (mainly carboxylates) are exposed to the aqueous environment. This way, the self-assembly yields particles that encapsulate within them the ICG associated with the hydrophobic core via hydrophobic interaction, as illustrated in Figure 9.

7.4. Optimization of the ICG concentration entrapped within the Prot8 particles

In order to optimize the particles fluorescence intensity, different concentration (0.5, 1, 2 and 5% w/w relative to Prot8) of ICG were added to the Prot8 hot solution, prior to the formation of the particles through the self-assembly process, as described above. The NIR fluorescent

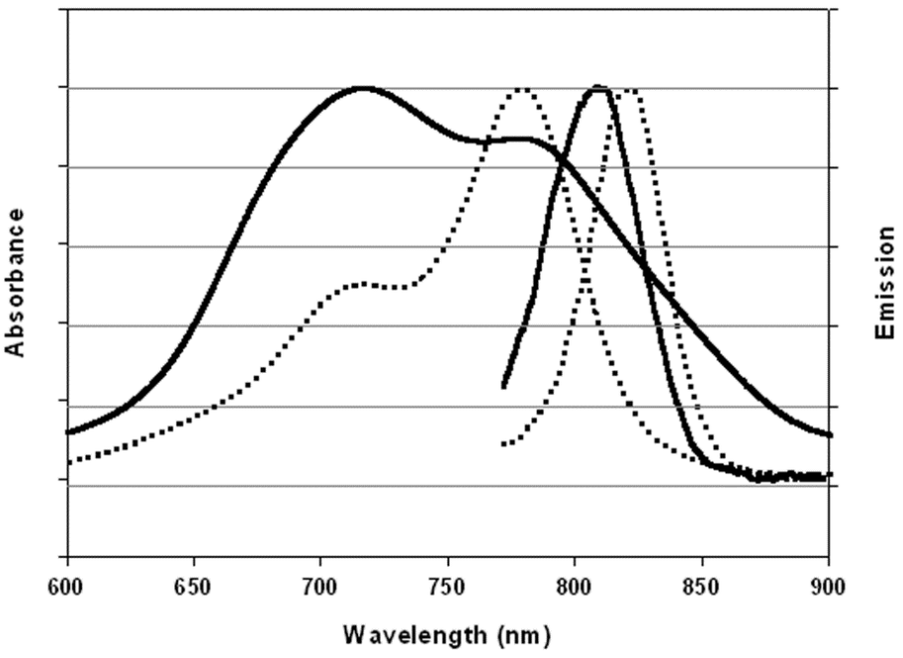

Figure 8. Absorbance and emission spectra of free ICG (dotted lines) and ICG-encapsulated Prot8 particles (solid lines) dispersed in water.

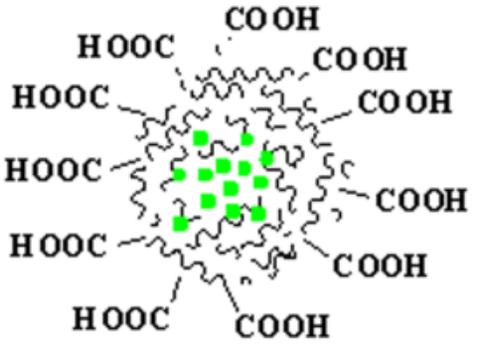

Figure 9. Schematic representation of the self-assembled NIR fluorescent particles. Hydrophobic moieties are represented by scribbled lines, ICG is represented by the interior green dots.

Prot8 particles dispersed in PBS were diluted to 1 mg/mL and their fluorescence intensities were measured at 809 nm. The encapsulated ICG concentration that gave the maximum fluorescence intensity of the resultant NIR fluorescent particles was 1% w/w relative to Prot8. At higher dye concentrations, quenching of the fluorescence was observed, as the dye molecules encapsulated within the Prot8 nanoparticle are close to each other, resulting in non-emissive energy transfer between them.

7.5. Photostability of the NIR fluorescent Prot8 particles

In order to examine the photostability of the encapsulated ICG as opposed to free ICG, photobleaching experiments were performed for both the encapsulated and the free dye. For this purpose, an aqueous solution of ICG (0.05 M) in PBS was prepared, and the

fluorescence intensity with λex set at 780 nm and λem set at 800 nm was measured. A dispersion of NIR fluorescent Prot8 particles in PBS was prepared, and diluted to give similar fluorescence intensity to the dye at the same wavelengths. The excitation and emission slits were opened to 20 nm and 5 nm, respectively. Each of the samples was illuminated continuously with a xenon lamp, and the fluorescence intensity was measured over a period of 20 min by a Cary Eclipse fluorescence spectrophotometer (Agilent Technologies Inc.). Intensity values were normalized for comparison. Figure 10 illustrates that during illumination, the fluorescence intensity of the ICG-containing Prot8 particles remains intact while that of the free ICG decreased significantly. The photobleaching of ICG is significantly reduced by the encapsulation within the proteinoid-PLLA particles. The encapsulation probably protects the free dye from light-inducing factors such as oxygen, oxidizing or reducing agents, temperature, exposure time and illumination levels, which may reduce the fluorescence intensity irreversibly [58,59].

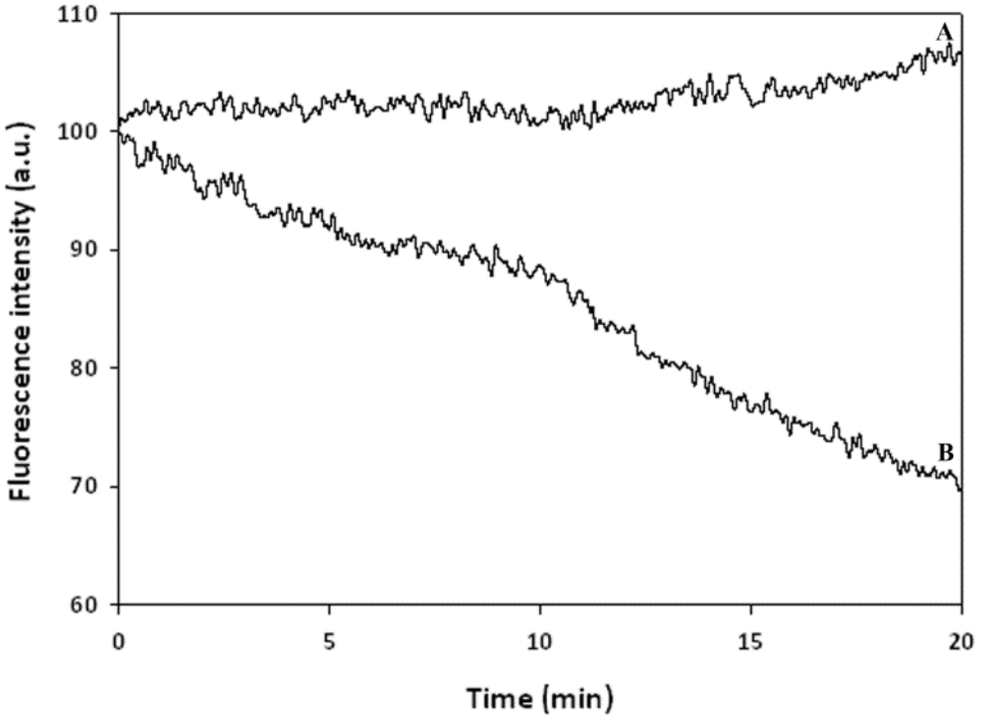

Figure 10. Photostability of the ICG-containing Prot8 particles (A) and free ICG (B) as function of time. Samples of ICG-containing Prot8 particles and free ICG were illuminated with a Xenon flash lamp for 20 min, as described above.

7.6. In vitro cytotoxicity of the Prot8 particles

In order to revoke cell toxicity of the NIR Prot8 particles, in vitro cytotoxicity of the particles was tested by using human colorectal adenocarcinoma LS174t, SW480 and HT29 cell lines. The cell lines are adherent to the used culture dishes. LS174t cells were grown in Minimum

Essential Medium (MEM) eagle supplemented with heat-inactivated fetal bovine serum (FBS, 10%), penicillin (100 IU/mL), streptomycin (100 μg/mL) and L-glutamine (2 mM). SW480 cells were maintained in Dulbecco's MEM supplemented with heat-inactivated fetal bovine serum (FBS, 10%), penicillin (100 IU/mL), streptomycin (100 μg/mL) and L-glutamine (2 mM). HT29 cells were maintained in McCoy's 5A medium supplemented with FBS (10%), penicillin (100 IU/mL), streptomycin (100 μg/mL) and L-glutamine (2 mM). Cells were screened to ensure they remained mycoplasma-free using Mycoplasma Detection Kit [54]. Cell cytotoxicity was assessed by measuring the release of cytoplasmic lactate dehydrogenase (LDH) as described above.

Figure 11 exhibits the cytotoxicity levels of the Prot8 particles at two different concentrations (1.25 and 2.5 mg/mL). It can be seen that at both concentrations, the Prot8 particles have no significant cytotoxic effect on all three cell lines, compared to untreated (blank) cells, meaning that the particles may be used for biomedical applications as suggested, including drug delivery.

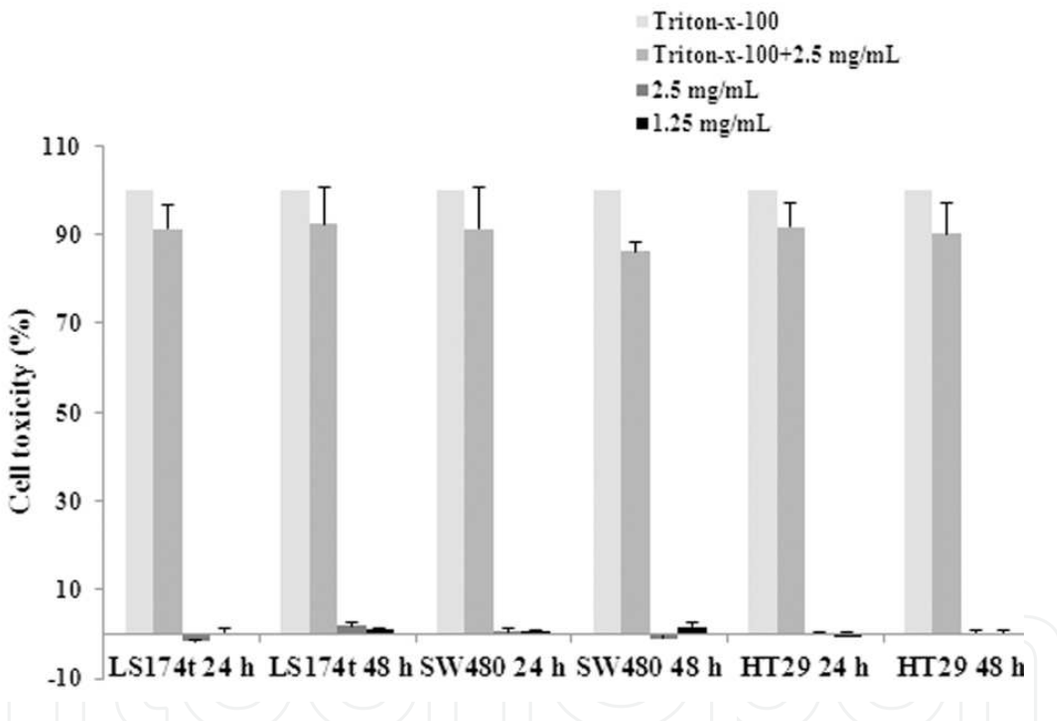

Figure 11. Cytotoxic effect of the NIR fluorescent Prot8 particles on human colorectal adenocarcinoma LS174t, SW480 and HT29 cell lines measured by the LDH assay. Cells (3×10^5) were incubated for 24 and 48 h with the Prot8 particles (1.25 and 2.5 mg/mL in PBS). Cells were incubated with 1% Triton-x-100 as positive control (100% toxicity). In addition, cells were incubated with Triton-x-100 1% and the Prot8 particles (2.5 mg/mL) to revoke any interaction of the particles with the LDH kit components. Untreated cells (negative control) were similarly incubated. Each bar represents mean ± standard deviations of 4 separate samples (originally published in [23]).

7.7. In vivo biodistribution in a mouse model

In order to examine the biodistribution in a living body, the NIR fluorescent Prot8 particles (2 mg/mL, 0.01 mg/kg body weight per mouse) were injected i.v. into mice through the tail vein

and checked at several time intervals over 24 h. Male BALB/C mice (Harlan Laboratories, Israel) were utilized in this study under a protocol approved by the Institutional Animal Care and Use Committee at Bar-Ilan University. The biodistribution of the NIR fluorescent Prot8 particles was studied in normal 8-weeks-old mice, weighing 20-25 g at the time of experiment. Prior to the experiment, mice were anesthetized by intraperitoneal injection of Ketamine (40-80 mg/kg body weight) and Xylazine (5-10 mg/kg body weight), and the mice's skin was shaved with an electric animal clipper.

100 μL of either nanoparticle dispersion or free ICG solution (0.01 mg/kg body weight, dissolved in PBS) were administered to the mice through tail vein injection at a concentration of 2 mg/mL. During image acquisition, mice remained anesthetized by the intraperitoneal injection of Ketamine/Xylazine. Image cubes were obtained from the mice at several time points up to 24 h after injection. Each treatment group includes 3 mice for each time point (5 min, 20 min, 1 h and 24 h); 2 uninjected mice served as negative control. The experiment was repeated twice, testing a total of 52 mice. At the end of the experiment, the mice were euthanized by cervical dislocation, and organs were taken for imaging (liver, spleen, kidney, duodenum, colon, brain, heart, tibia bone and blood).

Whole body fluorescence images were acquired using a Maestro II in vivo fluorescence imaging system (Cambridge Research &Instrumentation, Inc., Woburn, MA). The system is equipped with a fiber-delivered 300W xenon excitation lamp, and images can be acquired from λ=500-950 nm by a 1.3 megapixel CCD camera (Sony ICX285 CCD chip). Each pixel within the image cube therefore has an associated fluorescence spectrum. The software for the Maestro system (Maestro 2.10.0) contains several algorithms to process the spectral data cubes to remove undesired auto-fluorescence signal and generate overlaid images for multiple fluorophores. A deep red excitation/emission filter set was used for our experiments (λex: 700-770 nm, λem>780 nm). The liquid crystal tunable filter (LCTF) was programmed to acquire image cubes from λ=780 nm-860 nm with an increment of 10 nm per image. The camera was set to 150 ms (whole body image), 15 ms (liver), 500ms (spleen), 7000ms (kidney), 10 ms (duodenum), 500 ms (colon), 1000ms (brain), 1000ms (tibia bones), 200ms (heart) and 1000ms (blood) exposure times. Fluorescence intensity measurements were performed using ImageJ NIH (National Institutes of Health) software.

Figure 12 shows whole body images of mice injected with the particles over time: at 5 min, 20 min, 1 h and 24 h from injection. 5 min post injection, there is an initial burst of fluorescence which subsided quickly, while the majority of the fluorescent particles concentrated in the liver, at 20 min. 24 h post injection, the fluorescence is almost non-existent, signifying the nanoparticle clearance from the body over 24 h. Biodistribution was tested for free ICG as well, and no significant differences in distribution and kinetics were found between particles containing ICG and free ICG up to 24 h post injection. These findings were in complete agreement with previous reports of ICG and ICG-containing particles pharmacokinetics and biodistribution, as the free dye in solution, derivatives of the free dye and ICG-containing particles are all evacuated from the body after 1 h and completely vanished 24 h after i.v. injection [60,61].

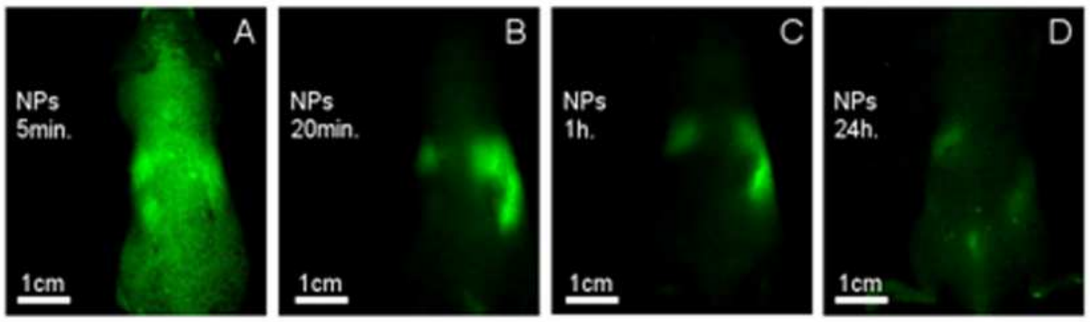

Figure 12. Typical whole body fluorescence images of the NIR fluorescent Prot8 particles at 5 min, 20 min, 1 h and 24 h after i.v injection. 12 mice (each experiment group contained 3 mice) were anesthetized and treated with NIR fluorescent Prot8 particles (2 mg/mL, 0.01 mg/kg body weight per mouse). Blood was drawn and organs were harvested at each time point. 2 uninjected mice served as negative control. 12 mice were injected correspondingly with free ICG solution, giving similar results (not shown). The experiment was repeated twice with similar results (originally published in [23]).

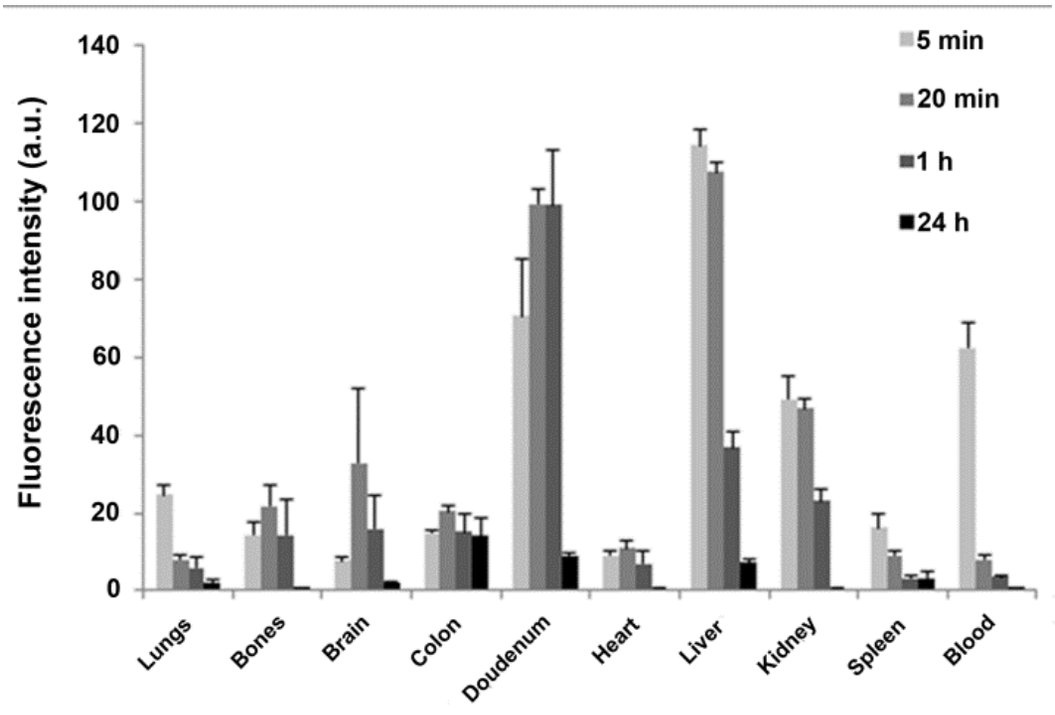

Figure 13. Fluorescence intensities of different organs taken at 5 min, 20 min, 1 h and 24 h post i.v. injection into mice tail veins. 12 mice (each experiment group contained 3 mice) were anesthetized and treated with NIR fluorescent Prot8 particles (2 mg/mL, 0.01 mg/kg body weight per mouse). Blood was drawn and organs were harvested at each time point. 2 uninjected mice served as negative control. The experiment was repeated twice with similar results (originally published in [23]).

Ex vivo fluorescence images of specific organs and blood were also obtained. Organs from mice were harvested and blood was drawn 5 min, 20 min, 1 h and 24 h post injection of the particles into the tail vein. Figure 13 shows the calculated fluorescence intensities of the lungs, bones, brain, colon, duodenum, heart, liver, kidney, spleen and blood screening. Evidently, this

analysis shows that the particles penetrated and were found in all checked organs. It is shown clearly that by 20 min most of the inserted quantity of the fluorescent particles is cleared from the blood. The particles concentrate mostly at the liver and are probably evacuated from the body. Interestingly, it is also apparent that the particles pass the blood-brain barrier (BBB), since they are found in the brain at 20 min post injection. This may open up a scope of drug targeting to the brain for drug molecules which are usually blocked. Overall, it was demonstrated that following a single i.v. injection of the particles, fluorescence intensity at all organs decreased over time, and only traces of fluorescence could be seen after 24 h.

7.8. Conjugation of the tumor-targeting ligands to the particles

PNA was covalently conjugated to the NIR fluorescent Prot8 particles by the cabodiimide activation method [62]. Briefly, EDC (1 mg) and Sulfo-NHS (1 mg) were each dissolved in 0.1 M MES (pH 6.0, 1 mL) containing 0.5 M NaCl. The EDC solution (1 mg/mL, 10 μL) was added to an aqueous solution of PNA (0.25 mg, 62.5 μL), followed by the addition of the sulfo-NHS solution (1 mg/mL, 25 μL). The mixture was then shaken for 15 min, followed by the addition of the NIR fluorescent Prot8 particles (2.5 mg in 1 mL PBS). The mixture was then shaken for 90 min. The obtained PNA-conjugated fluorescent particles were then washed from excess reagents by dilution and filtration through a 30-kDa filtration tube (VS2021 VIVA SPIN) at 1000 rpm (Centrifuge CN-2200 MRC) for 2 min, repeated three times. FITC–PNA, anti-CEA and anti-rabbit IgG were conjugated to the NIR fluorescent particles through a similar procedure. The concentration of bound PNA was determined with FITC–PNA by a calibration curve of FITC–PNA fluorescence using a multiplate reader (TECAN SpectraFluor Plus, Neotec Scientific Instruments). The concentrations of bound anti-CEA and anti-rabbit IgG were determined using a mouse IgG ELISA kit (Biotest, Israel). The calculated quantities of bound PNA and anti-CEA were 3.2 and 1.9 μg per mg particles, respectively.

7.9. Optical detection of human colon tumors in a chicken embryo model

7.9.1. The chicken embryo CAM model

A chicken embryo CAM model was used to test the specific tumor detection by both the non-conjugated and the bioactive (PNA, anti-CEA or anti-rabbit IgG) conjugated NIR fluorescent Prot8 particles. Among most commonly used animal models, the chicken egg model allows the imaging of several tumors in a short time period and is less expensive [62]. Tumor cells were grafted on CAM according to the literature [62,64]. Briefly, fertile chicken eggs obtained from a commercial supplier were incubated at 37°C at 60–70% humidity in a forced-draft incubator. On day 3 of incubation, an artificial air sac was formed, allowing the CAM to drop. After 8 days of incubation, a window was opened in the shell and the CAM was exposed. Tumor cells were collected by trypsinization, washed with culture medium and pelleted by gentle centrifugation. Following removal of the medium, 5x106 cells were resuspended in 30 μL ice-cold Matrigel and inoculated on the CAM at the site of the blood vessels. Eggs were then sealed and returned to incubation. On day 6 post-grafting, day 14 of incubation, the tumor diameter ranged from 3 to 5 mm with visible neoangiogenesis.

Figure 14 shows typical SW480 cell line derived tumors bordered by plastic rings on a chicken embryo CAM inside the egg.

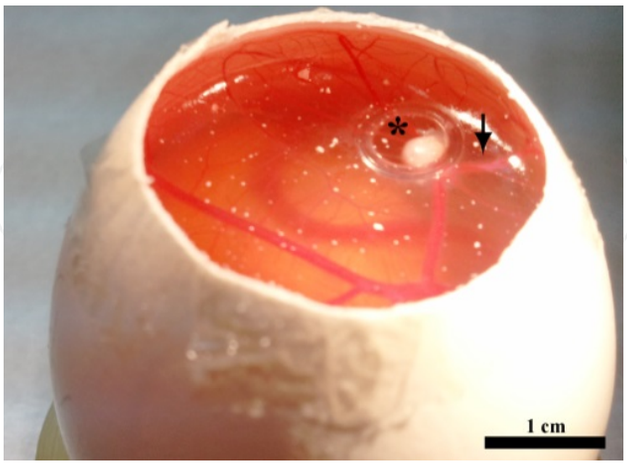

Figure 14. Light photograph of SW480 cell line derived tumors bordered by a plastic ring on chicken embryo CAM. Suspensions of 5×10^6 SW480 cells suspended in Matrigel formed compact structures (asterisk) 8 days after transplantation with attraction of host blood vessels (arrow).

7.9.2. CAM tumor detection

Chicken embryos with 6-days-old human adenocarcinoma tumors (LS174t and SW480 cancer cell lines) implanted on the CAM were treated with the non-conjugated, PNA-conjugated and anti-CEA-conjugated NIR fluorescent Prot8 particles (40 μL, 2 mg/mL). Additionally, non-pathological CAM treated with non-conjugated particles and untreated tumors served as control groups. After 40 minutes, the nanoparticle dispersions were removed and the tumors were washed with PBS. Then, the tumors and the non-pathological CAM were removed from the eggs, washed again with PBS and spread on a mat black background for observation using a Maestro II™ in vivo imaging system (Cambridge Research & Instrumentation, Inc., Woburn, MA). A NIR excitation/emission filter set was used for the experiments (λex: 710–760 nm, λem > 750 nm). The Liquid Crystal Tunable Filter (LCTF) was programmed to acquire image cubes from λ = 790 nm to 860 nm with an increment of 10 nm per image. Fluorescence intensity measurements were calculated as average intensity over the tumor surface area, using ImageJ software.

7.9.3. In vivo optical detection of human colon tumors in a CAM model

LS174t and SW480 colorectal cell lines were used to demonstrate the possible use of the NIR fluorescent Prot8 particles in tumor detection. As mentioned before, LS174t cells express certain receptors (β-D-galactosyl-(1-3)-N-acetyl-D-galactosamine and CEA) at a much higher extent than SW480 cells [62,65,66]. This way, the chosen bioactive ligands PNA and anti-CEA, once conjugated to the Prot8 particles, can lead the particles specifically to the LS174t cancer cells. As shown in Figure 15, the LS174t tumors treated with bioactive-conjugated particles (B and C) gained higher fluorescence than SW480 tumors, compared to those treated with non-

http://dx.doi.org/10.5772/59626

conjugated particles (A). This is accurate both for Prot8 particles conjugates with PNA (B) and anti-CEA (C), probably as a result of effective ligand-receptor interactions. In addition, the SW480 tumors treated with bioactive-conjugated Prot8 particles gained less fluorescence compared to those treated with the non-conjugated particles. The relative fluorescence intensities of the treated tumors by the conjugated and non-conjugated Prot8 particles are summarized in Figure 16. LS174t cells compared to SW480 cells gave fluorescence intensity ratios of 4:1 and 8:1 for PNA-conjugated particles and anti-CEA-conjugated particles, respectively. The non-conjugated Prot8 particles also labeled the tumors, however, the difference in the intensities between the types of tumors were not statistically significant. In this case, the overall fluorescence in both types of cells was higher than when treated with PNA-conjugated particles. This fact shows that even the bare non-conjugated particles penetrate the human cancer cell lines with a good extent. The possible reason is that the Prot8 particles can penetrate and label the cancerous cells specifically by either receptor-ligand interaction or utilization of these particles as nutrients for tumor growth, as they resemble biological proteins. The fluorescence intensity ratios between the types of cells show the significance of the nanoparticle surface. As seen in Figure 15D, no autofluorescence was observed in untreated tumors, signifying that all fluorescent signals are related to the fluorescent Prot8 particles labelling. Figure 15E shows that no non-specific labelling of non-pathological CAM tissue was observed, indicating the specificity of the Prot8 particles towards the tumor tissue.

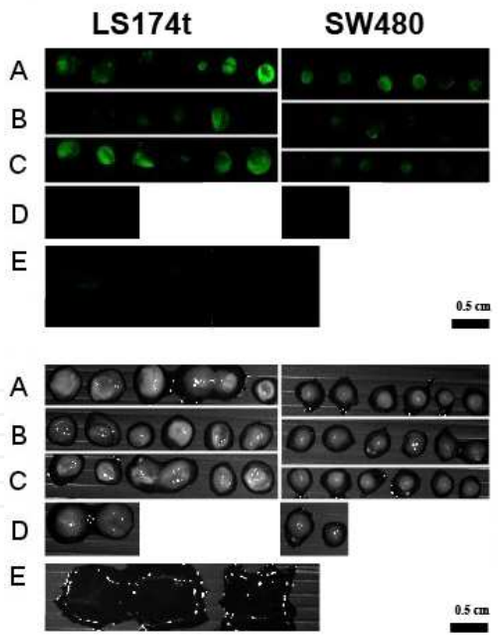

Figure 15. Fluorescent (upper) and greyscale (lower) images from a typical experiment of tumor cell lines LS174t and SW480 implants on chicken embryo CAM treated with non-conjugated (A), PNA-conjugated (B) and anti-CEA-conjugated (C) NIR fluorescent Prot8 particles. Images of untreated tumor cell lines are shown in (D). Images of non-pathological CAM treated with non-conjugated, PNA-conjugated and anti-CEA-conjugated particles are shown in (E). The experiment was repeated 5 times with similar results.

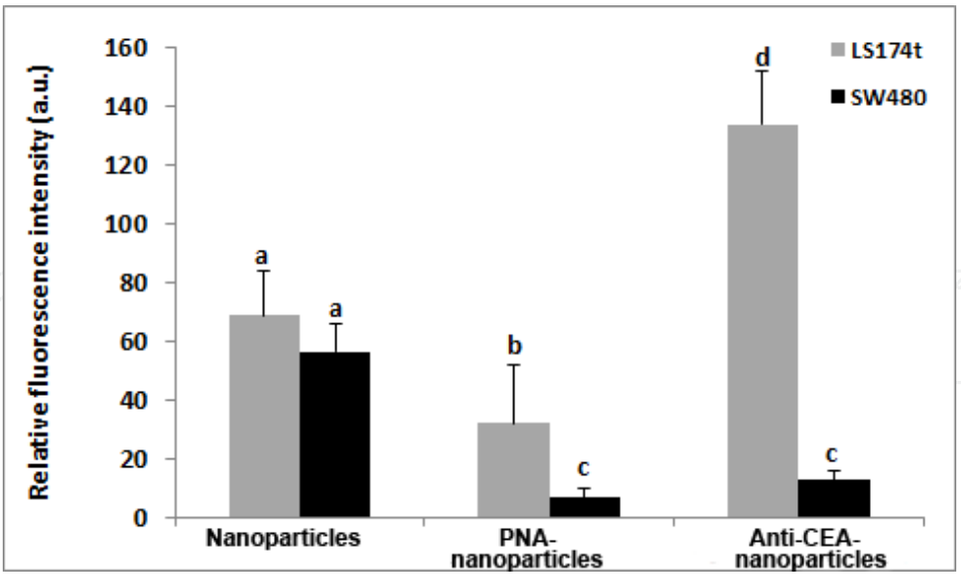

Figure 16. Relative fluorescence intensities of LS274t and SW480 tumors labeled with non-conjugated, PNA-conjugated and anti-CEA-conjugated particles. Data is presented as the mean value ± SE. Values not sharing a common letter (a, b, c or d) differ significantly from each other ($p<0.05$). The calculations are an average of 3 experiments.

In another set of *in vivo* experiments on LS174t and SW480 tumors implanted on the CAM model, the specific biomarker anti-CEA was tested against anti-rabbit IgG, serving as a non-specific agent, as well as a control group of non-conjugated particles. As clearly illustrated in Figure 17, LS174t tumors treated with anti-CEA-conjugated particles (B) gained greater fluorescence compared to those treated with non-conjugated particles (A) or anti-rabbit IgG-conjugated particles (C). This can be explained by the effective ligand-receptor interaction. Furthermore, the SW480 tumors treated with the anti-CEA-conjugated particles gained less fluorescence (about 3.5 times) compared to the LS174t tumors treated the same way. The fluorescent signal of LS174t tumors labeled by anti-CEA-conjugated particles was 4 times higher than that of the the tumors labeled by the anti-rabbit IgG-conjugated particles. Anti-rabbit IgG "blocks" the particle from interacting with the tumor receptors by the conjugation to the surface active moieties, thus serving as a negative control in colon tumor labelling.

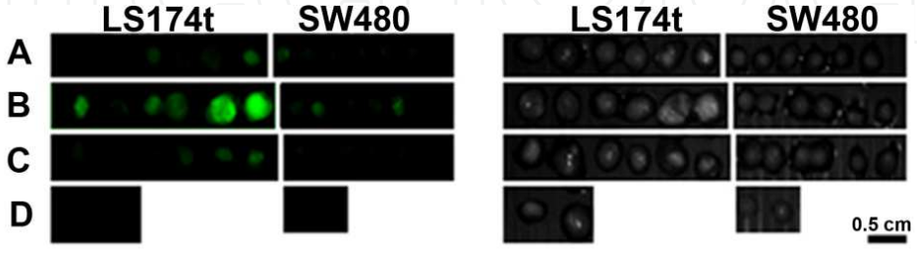

Figure 17. Fluorescent and grayscale images from a typical experiment of LS174t and SW480 human tumor cell lines implanted on chicken embryo CAM treated with the non-conjugated (A), anti-CEA-conjugated (B) and anti-rabbit IgG-conjugated (C) NIR fluorescent Prot8 particles. Images of untreated tumors are shown in (D). The experiment was repeated 3 times with similar results.

http://dx.doi.org/10.5772/59626

7.10. Optical detection of human colon tumors in a mouse model

Experiments were performed according to the protocols of the Israeli National Council for Animal Experiments by Harlan Biotech, Israel. Cancerous cells (30 μL containing 2×10^6 LS174t cells) were injected into the mouse intestinal wall. 2 weeks later the nude mice were anaesthetized and treated with the bio-conjugated NIR fluorescent Prot8 particles (0.1%, 200 μL), through the anus, using the guidance of a mini-colonoscope. 20 min later each colon was washed with PBS (5 × 1 mL) and mice were allowed to recover for 4 h. The mice were sacrificed and the colons were removed. Each colon was spread on a solid surface and imaging was performed using the Odysey Infra-red Imaging System (Li-Cor Biosciences, Lincoln, NE, USA) with excitation wavelength of 780 nm and emission wavelength of 800 nm.

Figure 18 shows typical (8 out of 10 mice) fluorescent and grayscale images of the mice colons after treatment with anti- CEA (A) and anti-rabbit IgG (B) conjugated particles. As illustrated in Figure 18A, the anti-CEA-conjugated particles detected the tumors specifically and selectively with good signal to background ratio (SBR), the background refers to the surrounding non-pathological tissue. Moreover, as illustrated in Figure 18B, the "inactive" anti-rabbit IgG-conjugated particles did not produce a significant signal of the tumors.

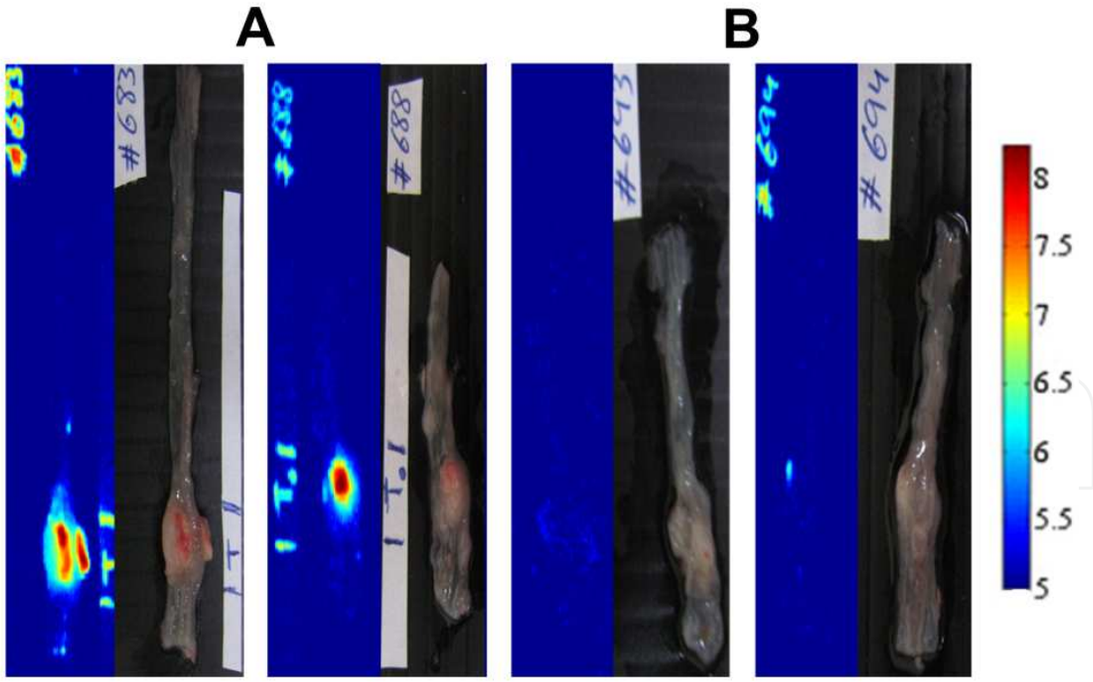

Figure 18. Fluorescent and grayscale images of typical LS174t colon tumors treated with anti-CEA (A) and anti-rabbit IgG (B)-conjugated NIR fluorescent Prot8 particles. 20 mice (10 in each experiment group) were anesthetized and treated with 0.1% particle dispersion in PBS, as described in section 3.2.5.14. 2 untreated mice served as a control group.

8. Summary and conclusions

In the present study, new proteinoids were prepared using L-glutamic acid, L-aspartic acid, L-phenylalanine, L-lysine and low molecular weight poly(L-lactic acid). The polymerization was carried out by a simple straight-forward condensation polymerization in heat. The optimal conditions for the polymerization were tested, including changing the temperature and using microwave radiation. The proteinoids made are of high molecular weights with narrow size distributions and possess optical activity, which can be later used in specific drug delivery using chirality. The proteinoids are thermally stable and each proteinoid has enough carboxylic acid and/or amine functional groups, which can be later used to bind covalently desired molecules, such as drugs and dyes. The incorporation of 2000 Da PLLA into the proteinoid backbone presented a stable proteinoid as well. Proteinoids were manipulated in several ways to give proteinoid sphere-shaped nano/micro-particles, and to optimize this process. Specific conditions were found for the production of hollow particles of narrow size distribution. The incorporation of PLLA segments into the proteinoids increased the hydrophobic interior part and resulted in smaller size hollow particles. The particles were found to be non-toxic and stable over time. Also, encapsulation of different materials was carried out, giving organic-filled particles and fluorescent particles. In summary, proteinoid formation and cytotoxicity tests indicate that these particles are suitable for further in vivo testing.

The copolymer Prot8 containing 10% PLLA, was chosen to be used for the biomedical study, since it provided the smallest particles with the biodegradability derived from the addition of PLLA to the proteinoid backbone. The proteinoid-PLLA copolymer was self-assembled in the presence of the NIR fluorescent dye ICG to yield NIR fluorescent Prot8 particles of 70 ± 15 nm dry diameter. These new NIR fluorescent particles were found to be stable, avoiding leakage and photobleaching of the NIR dye over time. Furthermore, these particles are non-toxic, as shown by LDH and XTT assays for cytotoxicity and cell viability on human colorectal adenocarcinoma cell lines. The particles biodistribution in a mouse model was tested, following an i.v. injection, and the results showed that the particles penetrate a variety of organs, including the brain and bones. Nevertheless, 1 h post injection, the particles concentrate at specific sites of the body and are evacuated almost completely over 24 h. It was established, using the chicken embryo CAM model and the tumor-implanted mouse model, that the NIR fluorescent particles may be very useful for tumor diagnosis in vivo due to their low auto-fluoresence of the background and the deep penetration into biomatrices. In the CAM model, when the NIR fluorescent proteinoid-PLLA particles are conjugated to a bioactive ligand (PNA or anti-CEA), they preserve their activity and specifically detect the cancer cells with upregulated receptors (LS174t vs. SW480). Non-conjugated and anti-rabbit IgG-conjugated NIR fluorescent particles (control particles) marked the cells without specific recognition at a much lower fluorescence intensity. In the mouse model, human tumor cells were implanted in mice colons, and the mice were treated with the NIR fluorescent particles. The results showed that the anti-CEA-conjugated particles specifically label the colon tumors, as opposed to those conjugated with anti-rabbit IgG antibodies.

In summary, the chapter introduced a new series of newly-made proteinoids of a narrow selection of amino acid monomers, with high molecular weight and very narrow polydispersity index. Furthermore, this chapter has described proteinoid fluorescent particles as potential probes for precancerous colorectal adenomatous polyps or colon cancer tumors. Selective and specific fluorescent labelling of tumors is possible, with very low background signal, however improvements are still necessary for optimizing the targeting efficiency of the particles. Recent and ongoing developments in fluorescence imaging systems will open up the scope for effective detection of fluorescently labelled neoplasm. The proteinoid particles may further be developed to serve for both diagnostics and therapy combined.

Author details

Michal Kolitz-Domb and Shlomo Margel*

*Address all correspondence to: shlomo.margel@mail.biu.ac.il

The Institute of Nanotechnology and Advanced Materials, Department of Chemistry, USA

References

[1] Fox SW. How did life begin? Science. 1960;132:200-8.

[2] Fox SW. Proteinoid theory of origin of life and competing ideas. The American Biology Teacher. 1974;36(3):161-72.

[3] Fox SW. Thermal synthesis of amino-acids and the origin of life. Geochimica et Cosmochimica Acta. 1995;59(6):1213-4.

[4] Fox SW, Jungck JR, Nakashim T. From proteinoid microsphere to contemporary cell - formation of internucleotide and peptide-bonds by proteinoid particles. Origins of Life and Evolution of Biospheres. 1974;5(1-2):227-37.

[5] Fox SW, Mccauley RJ, Fukushim T, Windsor CR, Montgome PO. Selective action in boundaries of particles of thermal proteinoid. Federation Proceedings. 1967;26(2):749.

[6] Fox SW, Nakashima T, Przybylski A, Syren RM. The updated experimental proteinoid model. International Journal of Quantum Chemistry. 1982:195-204.

[7] Fox SW, Waehneld TV. Thermal synthesis of neutral and basic proteinoids. Biochimica et Biophysica Acta. 1968;160(2):246-9.

[8] Fox SW, Harada K. Thermal copolymerization of amino acids to a product resembling protein. Science. 1958;128:1214.

[9] Fox SW, Harada K. The thermal copolymerization of amino acids common to protein. Journal of the American Chemical Society. 1959;82(14):3745–51.

[10] Fox SW, Harada K. Thermal copolymerization of amino acids in the presence of Phosphoric Acid. Archives of Biochemistry and Biophysics. 1960;86:281-5.

[11] Fox SW, Harada K. Thermal polymerization of amino acid mixtures containing Aspartic Acid or a thermal precursor of Aspartic Acid. United States patent 3,052,655. 1962.

[12] Fox SW, Harada K. Method of making copolymers of amino acids containing Glutamic Acid. United States patent 3,076,790. 1963.

[13] Harada K, Fox SW. The thermal condensation of Glutamic Acid and Glycine to linear peptides. Journal of the American Chemical Society. 1957;80(11):2694–7.

[14] Harada K, Matsuyama M. Polycondensation of thermal precursors of amino-acids and characterization of constituent amino-acids. Biosystems. 1979;11(1):47-53.

[15] Slager J, Domb AJ. Biopolymer stereocomplexes. Advanced Drug Delivery Reviews. 2003;55(4):549-83.

[16] Kohn J, Langer R. Polymerization reactions involving the side-chains of Alpha-L-Amino Acids. Journal of the American Chemical Society. 1987;109(3):817-20.

[17] Matsuno K. Electrical excitability of proteinoid microspheres composed of basic and acidic proteinoids. Biosystems. 1984;17(1):11-4.

[18] Przybylski AT. Excitable cell made of thermal proteinoids. Biosystems. 1985;17(4): 281-8.

[19] Przybylski AT, Fox SW. Excitable artificial cells of proteinoid. Applied Biochemistry and Biotechnology. 1984;10:301-7.

[20] Quirk S. Enhanced catalytic activity from proteinoid microspheres. Journal of Biomedical Materials Research Part A. 2013;101A(4):1133-43.

[21] Quirk S. Triggered release from proteinoid microspheres. United States patent 02314400 A1. 2007.

[22] Steiner S, Rosen R. Delivery systems for pharmacological agents encapsulated with proteinoids. Washington, USA patent 4,925,673. 1990.

[23] Kolitz-Domb M, Grinberg I, Corem-Salkmon E, Margel S: Engineering of near infrared fluorescent proteinoid-poly (L-lactic acid) particles for in vivo colon cancer detection. Journal of nanobiotechnology. 2014;12:1-13.

[24] Auras R. Poly (lactic acid). In: Encyclopedia Of Polymer Science and Technology.Wiley Interscience; 2010.

[25] Kulkarni R, Moore E, Hegyeli A, Leonard F. Biodegradable poly (lactic acid) polymers. Journal of Biomedical Materials Research Part A. 1971;5(3):169-81.

[26] Bala I, Hariharan S, Kumar M. PLGA nanoparticles in drug delivery: The state of the art. Critical Reviews in Therapeutic Drug Carrier Systems. 2004;21(5):387-422.

[27] Danhier F, Ansorena E, Silva JM, Coco R, Le Breton A, Préat V. PLGA-based nanoparticles: an overview of biomedical applications. Journal of Controlled Release. 2012;161(2):505-22.

[28] Dibbern E, Toublan FJJ, Suslick KS. Poly(glutamic acid) nanospheres for biomedical applications. Abstracts of Papers of the American Chemical Society. 2004;228:U346-U.

[29] Shikanov A, Kumar N, Domb AJ. Biodegradable polymers: An update. Israel Journal of Chemistry. 2005;45(4):393-9.

[30] Garlotta D. A literature review of poly (lactic acid). Journal of Polymers and the Environment. 2001;9(2):63-84.

[31] Tsuji H. Poly (lactic acid). In: Bio-Based Plastics: Materials and Applications. Kabasci S: John Wiley & Sons; 2013. 171-239.

[32] Lim LT, Auras R, Rubino M. Processing technologies for poly (lactic acid). Progress in Polymer Science. 2008;33(8):820-52.

[33] Bahn PR, Pappelis A, Bozzola J. Protocell-like microspheres from thermal polyaspartic acid. Origins of Life and Evolution of Biospheres. 2006;36(5-6):617-9.

[34] Milstein SJ, Kantor ML. Proteinoid Microspheres and Methods for Preparation and Use Thereof. United States patent 5,601,846. 1997.

[35] Bamnolker H, Nitzan B, Gura S, Margel S. New solid and hollow, magnetic and nonmagnetic, organic-inorganic monodispersed hybrid microspheres: synthesis and characterization. Journal of Materials Science Letters. 1997;16(16):1412-5.

[36] Syren RM, Sanjur A, Fox SW. Proteinoid microspheres more stable in hot than in cold water. Biosystems. 1985;17(4):275-80.

[37] Bae SK, Kim JD. Aggregation behaviors and their pH sensitivity of cholesterol-conjugated proteinoids composed of glutamic acid and aspartic acid matrix. Journal of Biomedical Materials Research Part A. 2003;64A(2):282-90.

[38] Kokufuta E, Sakai H, Harada K. Factors controlling the size of proteinoid microspheres. Biosystems. 1983;16(3-4):175-81.

[39] Urry DW, Peng SQ. Nonlinear mechanical force induced pKa shifts: Implications for efficiency of conversion to chemical energy. Journal of the American Chemical Society. 1995;117(32):8478-9.

[40] Kumar ABM, Rao KP. Preparation and characterization of pH-sensitive proteinoid microspheres for the oral delivery of methotrexate. Biomaterials. 1998;19(7-9):725-32.

[41] Steiner S, Rosen R. Delivery systems for pharmacological agents encapsulated with proteinods. United States patent 4,925,673. 1990.

[42] Tallawi M. Proteinoid/hydroxyapatite hybrid microsphere composites. Journal of Biomedical Materials Research Part B: Applied Biomaterials. 2011;96(2):261-6.

[43] Mullerherold U, Nickel G. The stability of proteinoid microspheres. Biosystems. 1994;33(3):215-20.

[44] Nakashima T. Metabolism of proteinoid microspheres. Topics in Current Chemistry. 1987;139:57-81.

[45] Quirk S. Triggered release of small molecules from proteinoid microspheres. Journal of Biomedical Materials Research Part A. 2009;91A(2):391-9.

[46] Quirk S. Triggered release from peptide-proteinoid microspheres. Journal of Biomedical Materials Research Part A. 2010;92A(3):877-86.

[47] Toublan FJJ, Dibbern E, Argadine HM, Greenleaf JF, Simari RD, Suslick KS. Electrostatic adhesion of polyelectrolytes and colloids on protein microspheres. Abstracts of Papers of the American Chemical Society. 2004;228:U350-U.

[48] Quirk S. Diagnostic signal amplification with proteinoid microspheres. U.S. patent 20030138975A1. 2003.

[49] Janairo G, Sy ML, Yap L, Llanos-Lazaro N, Robles J. Determination of the Sensitivity Range of Biuret Test for Undergraduate Biochemistry Experiments. e-Journal of Science and Technology. 2011;5:77-83.

[50] Harris FW. State of the art: Polymer chemistry. Introduction. Journal of Chemical Education. 1981;58(11):836.

[51] Dose K. Chemical and catalytical properties of thermal polymers of amino acids (proteinoids). Origins of Life. 1974;5(1-2):239-52.

[52] Heiskanen J. Comparison of three methods for determining the particle density of soil with liquid pycnometers. Communications in Soil Science and Plant Analysis. 1992;23(7-8):841-6.

[53] Ma XH, Santiago N, Chen YS, Chaudhary K, Milstein SJ, Baughman RA. Stability study of drug-loaded proteinoid microsphere formulations during freeze-drying. Journal of Drug Targeting. 1994;2(1):9-21.

[54] Epsztejn S, Glickstein H, Picard V, Slotki IN, Breuer W, Beaumont C, et al. H-ferritin subunit overexpression in erythroid cells reduces the oxidative stress response and induces multidrug resistance properties. Blood. 1999;94(10):3593-603.

[55] Decker T, Lohmannmatthes ML. A quick and simple method for the quantitation of Lactate-Dehydrogenase release in measurements of cellular cyto-toxicity and tumor necrosis factor (TNF) activity. Journal of Immunological Methods. 1988;115(1):61-9.

[56] Haritoglou C, Freyer W, Priglinger SG, Kampik A. Light absorbing properties of indocyanine green (ICG) in solution and after adsorption to the retinal surface—an ex-vivo approach. Graefe's Archive for Clinical and Experimental Ophthalmology. 2006;244(9):1196-202.

[57] Zweck J, Penzkofer A. Microstructure of indocyanine green J-aggregates in aqueous solution. Chemical Physics. 2001;269(1):399-409.

[58] Altınoğlu Eİ, Adair JH. Near infrared imaging with nanoparticles. Wiley Interdisciplinary Reviews Nanomedicine and Nanobiotechnology. 2010;2(5):461-77.

[59] Sharrna P, Brown S, Walter G, Santra S, Moudgil B. Nanoparticles for bioimaging. Advances in Colloid and Interface Science. 2006;123:471-85.

[60] Yaseen MA, Yu J, Jung B, Wong MS, Anvari B. Biodistribution of encapsulated indocyanine green in healthy mice. Molecular Pharmaceutics. 2009;6(5):1321-32.

[61] Mizrahi DM, Ziv-Polat O, Perlstein B, Gluz E, Margel S. Synthesis, fluorescence and biodistribution of a bone-targeted near-infrared conjugate. European Journal of Medicinal Chemistry. 2011;46(10):5175-83.

[62] Cohen S, Pellach M, Kam Y, Grinberg I, Corem-Salkmon E, Rubinstein A, et al. Synthesis and characterization of near IR fluorescent albumin nanoparticles for optical detection of colon cancer. Materials Science and Engineering: C. 2012;33:923-31.

[63] Durupt F, Koppers-Lalic D, Balme B, Budel L, Terrier O, Lina B, et al. The chicken chorioallantoic membrane tumor assay as model for qualitative testing of oncolytic adenoviruses. Cancer Gene Therapy. 2012;19(1):58-68.

[64] Noiman T, Buzhor E, Metsuyanim S, Harari-Steinberg O, Morgenshtern C, Dekel B, et al. A rapid in vivo assay system for analyzing the organogenetic capacity of human kidney cells. Organogenesis. 2011;7(2):140-4.

[65] Kaushal S, McElroy MK, Luiken GA, Talamini MA, Moossa A, Hoffman RM, et al. Fluorophore-conjugated anti-CEA antibody for the intraoperative imaging of pancreatic and colorectal cancer. Journal of Gastrointestinal Surgery. 2008;12(11):1938-50.

[66] Corem-Salkmon E, Perlstein B, Margel S. Design of near-infrared fluorescent bioactive conjugated functional iron oxide nanoparticles for optical detection of colon cancer. International Journal of Nanomedicine. 2012;7:5517-27.

IntechOpen